

Longitudinal Control of Vehicles in Traffic Microsimulation

Shirin Noei^{a,*}, Xilei Zhao^a, Carl D. Crane^b

^aDepartment of Civil and Coastal Engineering, University of Florida, Gainesville, FL 32611, USA

^bDepartment of Mechanical and Aerospace Engineering, University of Florida, Gainesville, FL 32611, USA

Abstract

Current state-of-art traffic microsimulation tools cannot accurately estimate safety, efficiency, and mobility benefits of automated driving systems and vehicle connectivity because of not considering physical and powertrain characteristics of vehicles and resistance forces. This paper proposes realistic longitudinal control functions for autonomous vehicles with and without vehicle-to-vehicle communications and a realistic vehicle-following model for human-driven vehicles, considering driver characteristics and vehicle dynamics. Conventional longitudinal control functions apply a constant time gap policy and use empirical constant controller coefficients, potentially sacrificing safety or reducing throughput. Proposed longitudinal control functions calculate minimum safe time gaps at each simulation time step and tune controller coefficients at each simulation time step during acceleration and deceleration to maximize throughput without compromising safety.

Keywords: vehicle dynamics, traffic microsimulation tool, longitudinal control, cooperative autonomous vehicle

1. Introduction

National Highway Traffic Safety Administration (NHTSA) identified driver errors as a critical reason for 94% of estimated 2,046,000 crashes (NHTSA, 2018a) with an estimated cost of \$836 billion (NHTSA, 2018b). Shifting responsibilities from a human driver to automated driving systems can increase safety and throughput (NHTSA, 2019).

NHTSA and Society of Automotive Engineers (SAE) defined six levels for vehicle automation. Advanced driving assistance systems assist Level 1 automated vehicles with steering or braking/acceleration and rely on human driver for all driving tasks. Cruise control, adaptive cruise control (ACC), and cooperative adaptive cruise control (CACC) are commercially available automated longitudinal control functions. Automated driving systems enable Level 5 automated vehicles to perform all driving tasks under any conditions without any intervention from a human driver.

Autonomous longitudinal control functions have limited sensing capabilities. Average data transmission delay for autonomous longitudinal control functions is 1.5 seconds per vehicle

*Corresponding author

Email address: shirinnoei@ufl.edu (Shirin Noei)

Table 1: State-of-art maximum acceleration and maximum deceleration values (ft/s²).

Author	Max. Acceleration	Max. Deceleration
Akçelik and Besley (2001)	8.8	10.1
Lemessi (2001)	8.2	8.2
Ahn et al. (2002)	10.1	NA
Rakha and Ding (2003)	4.9	8.2
Wang and Liu (2005)	8.2	11.5
Fang and Elefteriadou (2005)	4.9,6.9,8.2,9.2,11.5,15.1	9.8,15.1
Arasan and Koshy (2005)	2.6,2.7,4.9	NA
Kuriyama et al. (2010)	8.8	9.8
Song et al. (2012)	11.5	13.1
Shladover et al. (2012)	6.6	6.6
Lee and Park (2012)	13.1	9.8
Maurya and Bokare (2012)	NA	2.9,5.3
Lee et al. (2013)	10	15
Anyu et al. (2014)	1.5,8.5,9.8,11.1,19.1,22,25	3.7,16.4,19.7,23,36.7,44,51.5
Li et al. (2014)	4.5	11
Desiraju et al. (2014)	6.6	NA
Amoozadeh et al. (2015)	9.8	16.4
Bokare and Maurya (2017)	3.2,7.3,9.4	2.9,14.2,16.4
Ramezani et al. (2018)	8.2	9.8
Liu et al. (2018)	6.6	NA

length—from onboard sensors, data processing, control, and actuation—which prevents vehicles from closely following one another to form a string (Guo, 2017). Autonomous longitudinal control functions have a maximum range of about 50 meters to 200 meters due to relying entirely upon onboard sensors (Arem et al., 2007).

Vehicles with vehicle-to-vehicle (V2V) communications can follow their leaders at shorter gaps and with less variation in acceleration compared with vehicles with no external communications, potentially improving operational conditions, environmental factors, and safety—V2V-based warning technologies could help eliminate 4.5 million multi-vehicle crashes of 6.3 million police-reported crashes (NHTSA, 2017).

V2V communications improve situational awareness of autonomous vehicles, enabling autonomous vehicles to broadcast and receive omnidirectional messages—up to 10 times per second, creating a 360-degree awareness of surrounding vehicles in a range of 300 meters (Guo, 2017). Cooperative autonomous longitudinal control functions augment internal sensor data with data received—through DSRC and 4G-LTE—from surrounding vehicles. Most basic cooperative autonomous longitudinal functions depend on sharing of data, including position, speed, acceleration, deceleration, intentions, and performance limitations, between a vehicle and its immediate follower.

Autonomous vehicles must be demonstrated to be safe under a wide range of scenarios before they can be brought to market. Testing autonomous vehicles on public roads still pending adoption of safety standards and performance requirements and takes a considerable amount of time and effort. Using simulation tools can 1) boost speed of data collection to reach mileage accumulation while reducing fleet operation costs, and 2) add more diversity and complexity to

test scenarios.

Current state-of-art traffic microsimulation tools, such as Vissim, Aimsun, and INTEGRATION, enable users to model autonomous and cooperative autonomous vehicles. However, none of conventional traffic microsimulation tools provide users with a platform to model vehicle dynamics with a reasonable level of accuracy—there is a trade-off between speed of processing and accuracy. Vissim does not take into account physical and powertrain characteristics of vehicles and resistance forces and should be integrated with other vehicle dynamics simulation tools, such as CarMaker, to model vehicle dynamics (PTV Vissim, 2019). Aimsun incorporates vehicle kinematics to estimate quantities of motion (Aimsun, 2019).

Vissim and Aimsun are not realistic in terms of considering constant values for maximum acceleration and maximum deceleration. Vissim considers maximum deceleration of 13.8 ft/s^2 as default (Lu et al., 2014). Aimsun considers maximum acceleration of 11.5 ft/s^2 and maximum deceleration of 13.1 ft/s^2 as default (Lu et al., 2014). Most microsimulation models also consider constant values for maximum acceleration and maximum deceleration (see Table 1). However, maximum acceleration and maximum deceleration are specific to vehicle characteristics and road conditions and change in real-time with speed.

Vissim (Arem et al., 2007), Aimsun (Arem et al., 2006), and microsimulation models (Liu et al., 2018; Milanés et al., 2013; Amoozadeh et al., 2015; Ramezani et al., 2018) consider constant time gaps and controller coefficients. Longer time gaps reduce throughput, shorter time gaps increase rear-end crashes, and constant controller coefficients cannot maximize throughput without compromising safety. Proposed longitudinal controller functions consider dynamic time gaps and controller coefficients to maximize throughput without compromising safety.

INTEGRATION assumes a constant value for engine-generated horsepower (Rakha et al., 2004). Some microsimulation models assume a linearly decreasing engine-generated horsepower in calculated maximum acceleration (Rakha and Lucic, 2002). However, engine-generated horsepower is specific to vehicle characteristics and changes in real-time with speed. Considering constant values for maximum acceleration, maximum deceleration, and engine-generated horsepower contributes to inaccurate estimation of safety, efficiency, and mobility benefits of automated driving systems and vehicle connectivity. This paper proposes a microsimulation tool that utilizes physical and powertrain—engine, transmission, and drivetrain—properties of vehicles, and resistance forces— aerodynamic, rolling, and grade—to determine maximum acceleration and maximum deceleration capabilities at each simulation time step.

This paper mainly 1) defines upper bounds for acceleration and deceleration, 2) defines lower bound for distance gap and time gap, 3) designs longitudinal control functions, and 4) tunes controller coefficients. Section 2 provides a microsimulation model to calculate maximum acceleration, maximum deceleration, minimum safe distance gap, and minimum safe time gap at each simulation time step based on physical and powertrain properties of vehicles and resistance forces. Section 3 introduces two criteria for tuning controller coefficients at each simulation time step during acceleration and deceleration based on vehicle dynamics to maximize throughput without compromising safety. Section 4 proposes a vehicle-following model for human-driven vehicles and longitudinal control functions for autonomous and cooperative autonomous vehicles, considering driver characteristics and vehicle dynamics. Section 5 verifies proposed vehicle-following model and longitudinal control functions for fourteen vehicle models, driving in manual, autonomous, and cooperative autonomous modes, over two driving schedules designed for aggressive—high speed and high acceleration—driving behavior.

2. Road Vehicle Performance

This section incorporates physical and powertrain properties of vehicles and resistance forces to calculate maximum acceleration (Mannering and Washburn, 2019), maximum deceleration, minimum safe distance gap, and minimum safe time gap for vehicles in a string.

2.1. Maximum Acceleration

Three significant sources of resistance against longitudinal movement of vehicles are aerodynamic resistance, rolling resistance, and grade resistance. Aerodynamic resistance can be calculated as:

$$R_a[k] = \rho C_D A_f v^2[k]/2, \quad (1)$$

where R_a is aerodynamic resistance (lb), $[k]$ denotes discrete-time variable—(t) denotes continuous-time variable, and Δt is simulation time step s.t. $t = k\Delta t$ —, ρ is air density (slug/ft³), C_D is drag coefficient, A_f is vehicle frontal area (ft²), calculated as vehicle width (ft) \times vehicle height (ft), and v is speed (ft/s). Rolling resistance can be approximated as:

$$R_{rl}[k] \approx f_{rl}[k]W, \quad (2)$$

where R_{rl} is rolling resistance (lb), f_{rl} is coefficient of rolling resistance, and W is weight (lb). For vehicles operating on paved surfaces, f_{rl} can be approximated as $0.01(1 + v[k]/147)$. Assuming angle of inclination is small, grade resistance can be approximated as:

$$R_g \approx WG, \quad (3)$$

where R_g is grade resistance (lb), and G is grade specified in percentage. G has a positive value for an upward slope and a negative value for a downward slope. Tractive effort available to overcome resistance and to provide acceleration is taken as lesser of maximum tractive effort and engine-generated tractive effort. Maximum tractive effort can be approximated as:

$$F_{max}[k] \approx \begin{cases} \mu W (l_r + h f_{rl}[k]) / (L + \mu h) & \text{front-wheel-drive,} \\ \mu W (l_f - h f_{rl}[k]) / (L - \mu h) & \text{rear-wheel-drive,} \\ \mu W & \text{all-wheel-drive,} \end{cases} \quad (4)$$

where F_{max} is maximum tractive effort (lb), μ is coefficient of road adhesion, l_r is distance from rear axle to center of gravity (ft), h is height of center of gravity above road surface (ft), L is length of wheelbase (ft), and l_f is distance from front axle to center of gravity (ft). For vehicles with low power-to-weight ratio, such as commercial trucks, maximum acceleration is based on engine-generated tractive effort. Engine speed can be calculated as:

$$n_e[k] = v[k]\epsilon_0[k]/[2\pi r(1 - i)], \quad (5)$$

where n_e is engine speed (revs/s), ϵ_0 is overall gear reduction ratio, calculated as transmission gear ratio (selected based on speed) \times differential gear ratio, r is radius of drive wheels (ft), and i is slippage of driver axle. Note that engine speed for stopped vehicles is a function of throttle input. Engine-generated horsepower can be calculated as:

$$hp_e[k] = 2\pi M_e[k]n_e[k]/550, \quad (6)$$

where hp_e is engine-generated horsepower (hp)—1 horsepower equals 550 ft-lb/s—, and M_e is torque (ft-lb)—torque can be determined from torque map (see Figure 11). Engine-generated tractive effort reaching drive wheels can be calculated as:

$$F_e[k] = M_e[k]\epsilon_0[k]\eta_d/r, \quad (7)$$

where F_e is engine-generated tractive effort (lb), and η_d is mechanical efficiency of drivetrain. Based on Newton's first law of motion, maximum acceleration can be approximated as:

$$a_{max}[k] \approx (F[k] - \sum R[k]) / (m\gamma_m[k]), \quad (8)$$

where a_{max} is maximum acceleration (ft/s²), $F[k] = \min(F_{max}[k], F_e[k])$, $\sum R[k] = R_a[k] + R_{rl}[k] + R_g$, m is mass (slugs), and γ_m is mass factor accounting for moments of inertia during acceleration, approximated as $1.04 + 0.0025\epsilon_0^2[k]$.

2.2. Maximum Deceleration

Maximum braking force can be approximated as:

$$B_{max}[k] \approx \begin{cases} \eta_b\mu W [l_r + h(\mu + f_{rl}[k])] / L & \text{front-wheel-drive,} \\ \eta_b\mu W [l_f - h(\mu + f_{rl}[k])] / L & \text{rear-wheel-drive,} \\ \eta_b\mu W & \text{all-wheel-drive,} \end{cases} \quad (9)$$

where B_{max} is maximum braking force (lb), and η_b is braking efficiency. Maximum deceleration can be approximated as:

$$d_{max}[k] \approx (B_{max}[k] + \sum R[k]) / (m\gamma_b), \quad (10)$$

where d_{max} is maximum deceleration (g), and γ_b is mass factor accounting for moments of inertia during brake.

2.3. Minimum Safe Distance Gap

Minimum distance gap required to avoid a collision, assuming no aerodynamic resistance and a constant speed during sensing delay, communication delay, and actuation lag, can be calculated as:

$$S_{min}[k] = (\tau_s^{i+1} + \tau_c^{i+1} + \tau_{lag}^{i+1}[k]/2) v_{i+1}[k] - \tau_{lag}^i[k] v_i[k] / 2, \quad (11)$$

where S_{min} is minimum safe distance gap (ft), τ_s is sensing delay (s), τ_c is communication delay (s), τ_{lag} is lag in tracking desired deceleration (s), calculated as $v[k]/d_{max}[k]$, and subscripts/superscripts $i + 1$ and i denote subject vehicle and its leader, respectively.

2.4. Minimum Safe Time Gap

Minimum time gap required to avoid a collision can be further calculated as:

$$T_{min}[k] = \tau_s^{i+1} + \tau_c^{i+1} + \tau_{lag}^{i+1}[k] - \tau_{lag}^i[k], \quad (12)$$

where T_{min} is minimum safe time gap (s).

3. Control Design

Consider a standard ACC (Figure 1), consisting of a lower-level controller and an upper-level controller. Upper-level ACC determines desired acceleration, and lower-level ACC determines throttle input required to track desired acceleration. Upper-level ACC can be modeled as:

$$\begin{cases} a_{i+1}(t) = K_p e_v(t) + K_d a_i(t) & \text{time domain,} \\ A_{i+1}(s) = A_i(s) - \tau_{lag}^{i+1} J_{i+1}(s) & s \text{ domain,} \end{cases} \quad (13)$$

where a is acceleration in time domain, K_p is proportional gain (s^{-1}), e_v is error in speed (ft/s), calculated as $v_i(t) - v_{i+1}(t)$, K_d is derivative gain, A is acceleration in s domain, s denotes complex frequency variable, τ is assumed to be a constant value, and J is jerk in s domain (ft/s^3). Substituting $J(s) = s^2 V(s)$ and $A(s) = sV(s)$ in Equation 13 results in:

$$V_{i+1}(s) (\tau_{lag}^{i+1} s^2 + s) = A_i(s), \quad (14)$$

where V is speed in s domain. Plant model—transfer function between desired acceleration $A_i(s)$ and actual speed $V_{i+1}(s)$ —and controller model—transfer function between speed difference $V_i(s) - V_{i+1}(s)$ and desired acceleration—of upper-level ACC can be further modeled as:

$$P(s) := V_{i+1}(s)/A_i(s) = 1/[s(\tau_{lag}^{i+1} s + 1)], \quad (15)$$

$$C(s) := A_i(s)/[V_i(s) - V_{i+1}(s)] = K_p + K_d s, \quad (16)$$

where $P(s)$ is plant model, and $C(s)$ is PD controller model.

Definition 1. $H(s) = P(s)C(s)/[1 + P(s)C(s)]$ is closed-loop transfer function, assuming $P(s)$ as plant transfer function and $C(s)$ as controller transfer function.

A standard ACC with $P(s)$ as of Equation 15 and $C(s)$ as of Equation 16 has following closed-loop transfer function (see Definition 1):

$$H(s) = (K_p + K_d s) / (\tau_{lag}^{i+1} s^2 + (K_d + 1)s + K_p), \quad (17)$$

where $H(s)$ is closed-loop transfer function.

Definition 2. Consider step response—system output in response to a step input $u(t)$ —of a BIBO (bounded-input, bounded-output), stable, and proper system is in form of $H(s) = N(s)/D(s)$ —order of $D(s)$ is greater or equal to order of $N(s)$. Steady-state value of $H(s)$ can be calculated as $cH(0)$, where $u(t) = c \times 1(t)$, c is a constant value, and $H(0)$ is DC gain.

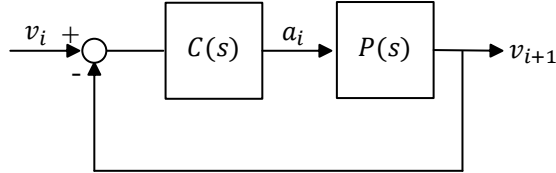


Figure 1: A standard adaptive cruise control.

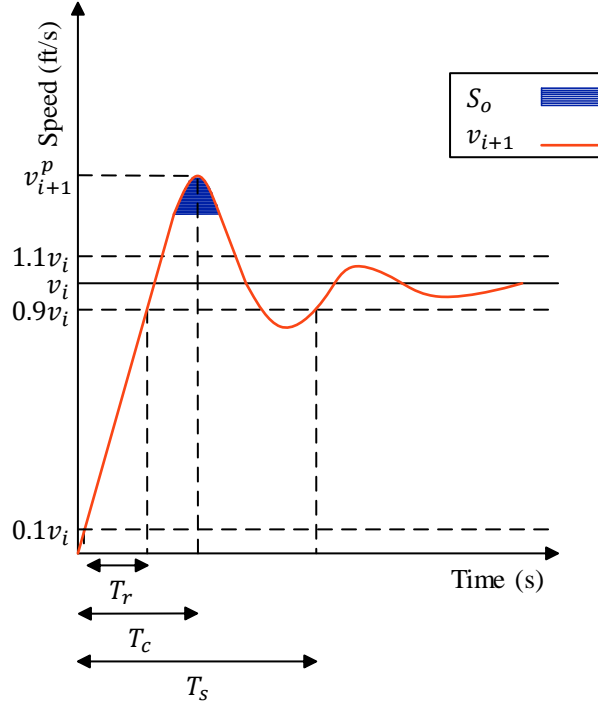


Figure 2: Various parameters used to characterize step response of a system.

Definition 3. Rise time (T_r) is a time it takes for a step response rising from 0.1 to 0.9 of its final value. Percent peak overshoot is peak value minus steady-state value, expressed as a percentage of steady-state value. 10% settling time (T_s) is the shortest time taking for a step response to enter a band of ± 10 of its final value and stay in that band after that (Figure 2).

Among four control types to be considered, i.e., proportional (P), proportional-integral (PI), proportional-derivative (PD), and proportional-integral-derivative (PID), PD controller is preferred since it results in a second-order closed-loop transfer function which is easier to be evaluated mathematically. Step response of $H(s)$ should have minimum rise time, overshoot, settling time, and steady-state error—desired value minus steady-state value—to ensure safety.

Definition 4. A strict left half-plane is part of s -plane, defined as $\{s \in \mathbb{C} | \text{Re}(s) < 0\}$.

Definition 5. Consider $H(s)=N(s)/D(s)$. Roots of $N(s)$ are called zeros of $H(s)$.

Excluding a strict left-half plane zero from $H(s)$ forms $G(s) = K_p / (\tau_{lag}^{i+1} s^2 + (K_d + 1) s + K_p)$. Assuming $G(s) = \omega_n^2 / (s^2 + 2\xi\omega_n s + \omega_n^2)$ results in:

$$\omega_n = \sqrt{K_p / \tau_{lag}^{i+1}}, \quad (18)$$

$$\xi = (K_d + 1) / (2 \sqrt{K_p \tau_{lag}^{i+1}}), \quad (19)$$

where ω_n is undamped natural frequency, and ξ is damping ratio.

Remark 1. Step response of a second-order closed-loop transfer function in form of $G(s) = \omega_n^2 / (s^2 + 2\xi\omega_n s + \omega_n^2)$ has following specifications:

$$T_r = \pi / (2\omega_n), \quad (20)$$

$$T_s = 4 / (\xi\omega_n), \quad (21)$$

$$v_p = \exp\left(-\pi\xi / \sqrt{1 - \xi^2}\right), \quad (22)$$

$$T_c = \pi / \left(\omega_n \sqrt{1 - \xi^2}\right), \quad (23)$$

where v_p is peak speed during overshoot, and T_c is peak time.

Following two conditions must be satisfied to maximize throughput without compromising safety:

$$\begin{cases} T_s < T_{min} & \text{during deceleration,} \\ S_o < S_{min} & \text{during acceleration,} \end{cases} \quad (24)$$

where T_s is settling time (s), S_o is distance traveled during overshoot (ft), approximated as $(T_c - T_r)(v_p^{i+1} - v^i)$ (shaded area in Figure 2), T_c is peak time (s), T_r is rise time (s), and v_p is peak speed during overshoot (ft/s).

Remark 2. Step response of $H(s)$ has lower rise time, not significantly different settling time, lower peak time, higher overshoot, and consequently not significantly different distance traveled during overshoot in comparison with step response of $G(s)$ for $K_p/K_d > 0$.

Since step response of $H(s)$ does not have significantly different settling time and distance traveled during overshoot compared with step response of $G(s)$ for $K_p/K_d > 0$ (see Remark 2), if step response of $G(s)$ meets safety requirements of Equation 24, step response of $H(s)$ also meet those requirements.

Remark 3. Laplace transform maps a function of continuous-time variable $f(t)$ to a function of complex frequency variable $F(s)$, where $s = \sigma + j\omega$, σ is real part of s , and ω is imaginary part of s . Z-transform maps a function of discrete-time variable $f[k]$ to a function of complex frequency variable $F(z)$, where $z = \sqrt{\sigma^2 + \omega^2} \exp(\sigma + j\omega)$.

Solving Equation 24 for K_p and K_d results in (see Remark 1):

$$K_d(t) < T_{min}(t) / (8\tau_{lag}^{i+1}) - 1, \quad (25)$$

$$\begin{aligned} & \left[2\pi\tau_{lag}^{i+1} / \sqrt{4K_p(t)\tau_{lag}^{i+1} - (K_d(t) + 1)^2} - \pi\sqrt{\tau_{lag}^{i+1} / (4K_p(t))} \right] \\ & \times \left[\exp\left(-\pi(K_d(t) + 1) / \sqrt{4K_p(t)\tau_{lag}^{i+1} - (K_d(t) + 1)^2}\right) - v_i(t) \right] < S_{min}(t). \end{aligned} \quad (26)$$

K_d should satisfy Equation 25 during deceleration, and K_p and K_d should satisfy Equation 26 during acceleration to ensure maximize throughput without compromising safety.

$H(z)$ is hard to be implemented in a microsimulation tool due to having many parameters to be calibrated ($H(z)$ is a third-order transfer function), so all variables in this section were expressed in s domain and continuous-time instead of z domain and discrete-time.

4. Longitudinal Movement

This section employs driver characteristics—desired acceleration multiplier, desired deceleration multiplier, and desired speed multiplier—and vehicle dynamics—maximum acceleration, maximum deceleration, minimum safe distance gap, and minimum safe time gap—in designing a vehicle-following model for human-driven vehicles and longitudinal control functions for autonomous and cooperative autonomous vehicles.

4.1. Human Driver Model

Human-driven vehicles are assumed to have 2D-IIDM (two dimensional improved intelligent driver model) (Tian et al., 2016) vehicle-following model but considering driver characteristics and vehicle dynamics in calculated maximum acceleration, maximum deceleration, and maximum speed. An important underlying assumption for human-driven vehicles is that drivers tend to be more conservative at higher speeds (Tian et al., 2016):

$$a_{i+1}[k] = \begin{cases} n \times a_{max}^{i+1}[k] C_s[k] C_v[k] & S[k] \geq S_{min}[k], \\ -q \times d_{max}^{i+1}[k] & \text{else,} \end{cases} \quad (27)$$

where n is desired acceleration multiplier, C_s is coefficient on distance gap, calculated as $1 - S_{min}^\alpha[k]/S^\alpha[k]$, S is distance gap (ft), calculated as $x_i[k] - x_{i+1}[k] - L_i$, x is front bumper position (ft), C_v is coefficient on speed, calculated as $1 - v_i^\beta[k]/(w \times FFS)^\beta$, w is maximum speed multiplier, FFS is free-flow speed (ft/s), q is desired deceleration multiplier, and α and β are constant tunable parameters adjusted in model calibration. IDM is easier to be calibrated and demonstrates a more stable performance compared with Wiedemann model (Zhu et al., 2018)—vehicle-following model used in Vissim.

4.2. Autonomous Longitudinal Control Function

In case when no leader is detected, a longitudinal P controller (similar to cruise control) is proposed:

$$a_{i+1}[k] = \max\left(\min\left(K_{p1}[k](FFS - v_{i+1}[k]), a_{max}^{i+1}[k]\right), -d_{max}^{i+1}[k]\right), \quad (28)$$

where K_{p1} is proportional gain (s^{-1}), and consequently $v_{i+1}[k+1] = a_{i+1}[k]\Delta t + v_{i+1}[k]$, and $x_{i+1}[k+1] = a_{i+1}[k]\Delta t^2/2 + v_{i+1}[k]\Delta t + x_{i+1}[k]$. Cruise control in Vissim is modeled as Equation 28 without considering maximum acceleration, maximum deceleration, and dynamic values for controller coefficients (Arem et al., 2007).

In case when 1) an autonomous vehicle approaches a vehicle, 2) an autonomous vehicle with V2V communications approaches a vehicle not equipped with V2V communications, or 3) there is a significant discrepancy between onboard sensor measurements and data received through V2V communications, an autonomous longitudinal PD controller—similar to ACC—is proposed:

$$a_{i+1}[k] = \max\left(\min\left(K_{p2}[k]e_p[k] + K_{d1}[k]e_v[k], a_{max}^{i+1}[k]\right), -d_{max}^{i+1}[k]\right), \quad (29)$$

where K_{p2} is proportional gain (s^{-1}), K_{d1} is derivative gain, e_x is error in distance gap, calculated as $S_{des}[k] - S[k]$, $S_{des}[k] = \max(T_{set}, T_{min}[k-1])v_{i+1}[k-1]$, and T_{set} is constant preset time gap (s). Autonomous vehicles can only apply autonomous longitudinal control functions. ACC in Vissim is modeled as Equation 29 without considering maximum acceleration, maximum deceleration, minimum safe time gap, and dynamic values for controller coefficients (Arem et al., 2007).

4.3. Cooperative Autonomous Longitudinal Control Function

When an autonomous vehicle with V2V communications approaches another autonomous vehicle with V2V communications, a cooperative autonomous longitudinal PID controller (similar to CACC) is proposed:

$$a_{i+1}[k] = \max\left(\min\left(K_{p3}[k]e_v[k] + K_{i1}[k]e_x[k] + K_{d2}[k]a_i[k], a_{max}^{i+1}[k]\right), -d_{max}^{i+1}[k]\right), \quad (30)$$

where K_{p3} is proportional gain (s^{-1}), K_{i1} is integral gain (s^{-2}), and K_{d2} is derivative gain. It is assumed in this paper that cooperative autonomous vehicles can only apply cooperative autonomous longitudinal control functions. CACC in Vissim (Arem et al., 2007) and CACC in Aimsun (Arem et al., 2006) are modeled as Equation 30 without considering maximum acceleration, maximum deceleration, minimum safe time gap, and dynamic values for controller coefficients.

5. Model Verification

This section 1) selects two driving schedules to test proposed vehicle-following model and longitudinal control functions, and 2) illustrates maximum accelerations, maximum decelerations, time gaps, and speed profiles of proposed vehicle-following model and longitudinal control functions for fourteen vehicle models, driving in manual, autonomous, and cooperative autonomous modes, over selected driving schedules.

5.1. Driving Schedule

The U.S. Environmental Protection Agency (EPA) uses eight chassis dynamometer driving schedules to test vehicle emissions and fuel economy (EPA, 2017). US06 driving schedule—also referred to as “supplemental federal test procedure”—is developed to reflect aggressive driving behavior, representing an 8-mile route with an average speed of 48 ft/s, a maximum speed of 80.3 ft/s, a maximum acceleration of 12.3 ft/s², and duration of 596 seconds.

Heavy-duty urban dynamometer driving schedule—also referred to as “cycle D”—is developed to test heavy vehicles, representing a 5.6-mile route with an average speed of 18.9 ft/s, a maximum speed of 58 ft/s, a maximum acceleration of 6.4 ft/s², and duration of 1060 seconds. US06 driving schedule is designed for testing light-duty vehicles with higher accelerations—maximum of 12.3 ft/s² vs. 6.4 ft/s²—and higher decelerations—maximum of 10.1 ft/s² vs. 6.8 ft/s²—compared with heavy-duty urban dynamometer driving schedule which is designed for testing heavy-duty vehicles.

5.2. Test Scenario

Assume a 2006 Honda Civic Si, a 2008 Chevy Impala, a 1998 Buick Century, a 2004 Chevy Tahoe, a 2002 Chevy Silverado, a 1998 Chevy S10 Blazer, a 2011 Ford F150, a 2009 Honda Civic, a 2005 Mazda 6, a 2004 Pontiac Grand Am, a single-unit truck with PACCAR PX-7 engine, an intermediate semi-trailer with PACCAR MX-13 engine, an interstate semi-trailer with PACCAR MX-13 engine, and a double semi-trailer with PACCAR MX-13 engine, follow a 2006 Honda Civic Si, over US06 and heavy-duty urban dynamometer driving schedules, driving in manual, autonomous, and cooperative autonomous modes—vehicles in cooperative autonomous mode are assumed to share their physical and powertrain properties, in addition to their accelerations, to their immediate followers and estimate location and speed of their immediate leaders—, with given conditions in Table 2. Vehicles are assumed to drive in a single lane, and there is no cut-in or cut-out maneuver.

Table 2: Input parameters.

Parameter	Value	Unit	Parameter	Value	Unit
ρ^*	0.002378	slug/ft ³	Δt	0.1	s
G	0	-	$S_{des}[1]$	5	ft
μ^{**}	1	-	T_{set}	1.1 ^{##} , 0.6 ^{###}	s
l_r	$L/2$	-	$p[1]$	100 [@] , 0 ^{@@}	ft
Drivetrain Type	Front-Wheel-Drive	-	$v[1]$	0 ^{@@}	ft/s
η_b	0.95	-	$a[1]$	0 ^{@@}	ft/s ²
γ_b	1.04	-	$K_{p1}[1]$	1	s ⁻¹
τ_s	1 [#] , 0.6 ^{##} , 0 ^{###}	s	$K_{p2}[1]$	-1	s ⁻¹
τ_c	0.1	s	$K_{p3}[1]$	1	s ⁻¹
Driver Type	5 ^{***}	-	$K_{i1}[1]$	-1	-
α	2	-	$K_{d1}[1]$	1	s ⁻²
β	4	-	$K_{d2}[1]$	1	s ⁻²
FFS	110	ft/s	Range of Detection	300	m

* for 0 ft altitude, 59° F temperature, and 14.7 lb/in² pressure, ** for good and dry pavement, *** corresponding to $n = 0.975$, $q = 0.99$, and $w = 1$, # in manual mode, ## in autonomous mode, ### in cooperative autonomous mode, @ leader, @@ follower.

5.3. Maximum Acceleration

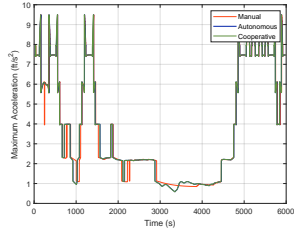
Maximum accelerations over US06 and heavy-duty urban dynamometer driving schedules are shown in Figure 3 and Figure 4, respectively, arranged from highest to lowest peak maximum acceleration value—2011 Ford F150 (9.5 ft/s²), 1998 Chevy S10 Blazer (9.1 ft/s²), 1998 Buick Century (9.1 ft/s²), 2004 Pontiac Grand Am (9 ft/s²), 2006 Honda Civic Si (8.8 ft/s²), 2005 Mazda 6 (8.7 ft/s²), 2009 Honda Civic (8.5 ft/s²), 2002 Chevy Silverado (8.4 ft/s²), 2008 Chevy Impala (8.4 ft/s²), intermediate semi-trailer (7 ft/s²), 2004 Chevy Tahoe (6.7 ft/s²), interstate semi-trailer (5.2 ft/s²), double semi-trailer (5 ft/s²), and single-unit truck (4.7 ft/s²).

Results show that 1) maximum acceleration is sensitive to vehicle model and driving schedule, 2) each vehicle model has a considerable range of maximum acceleration, 3) peak maximum acceleration value is irrespective of driving mode and driving schedule, 4) vehicles have equal maximum acceleration in autonomous and cooperative autonomous modes, and 5) trucks have lower maximum acceleration capabilities compared with passenger cars. Maximum acceleration is assumed to be zero for stopped vehicles and vehicles with constant speed.

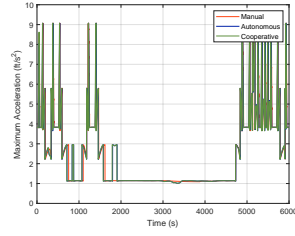
5.4. Maximum Deceleration

Maximum decelerations over US06 and heavy-duty urban dynamometer driving schedules are shown in Figure 5 and Figure 6, respectively, arranged from highest to lowest peak maximum deceleration value in manual mode over US06 driving schedule—2004 Chevy Tahoe (27.9 ft/s²), 2011 Ford F150 (26.8 ft/s²), single-unit truck (26.2 ft/s²), 2002 Chevy Silverado (26.1 ft/s²), 2009 Honda Civic (26 ft/s²), 1998 Chevy S10 Blazer (25.7 ft/s²), 2006 Honda Civic Si (25.6 ft/s²), 2005 Mazda 6 (25.4 ft/s²), 2004 Pontiac Grand Am (25.4 ft/s²), 2008 Chevy Impala (25.2 ft/s²), 1998 Buick Century (25.1 ft/s²), intermediate semi-trailer (21.3 ft/s²), interstate semi-trailer (20 ft/s²), and double semi-trailer (19.6 ft/s²).

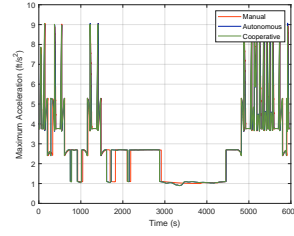
Results show that 1) maximum deceleration is sensitive to vehicle model and driving schedule, 2) each vehicle model does not have a considerable range of maximum deceleration, 3) peak



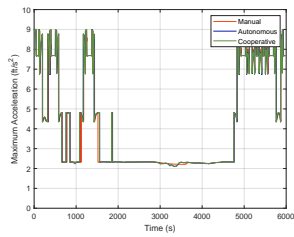
(a) 2011 Ford F150.



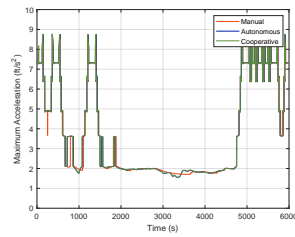
(b) 1998 Chevy S10 Blazer.



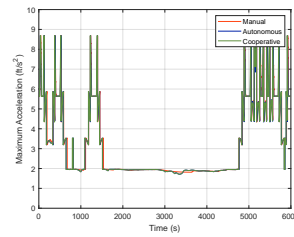
(c) 1998 Buick Century.



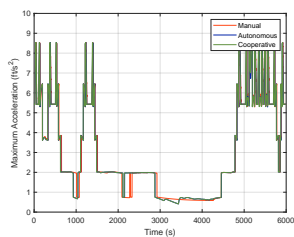
(d) 2004 Pontiac Grand Am.



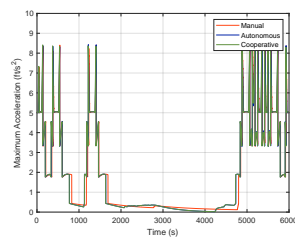
(e) 2006 Honda Civic Si.



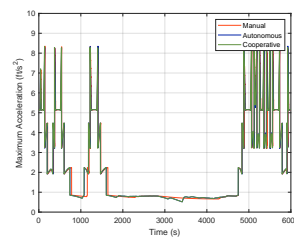
(f) 2005 Mazda 6.



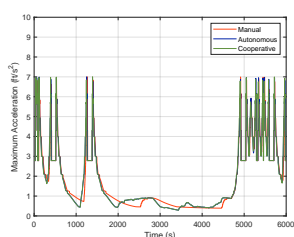
(g) 2009 Honda Civic.



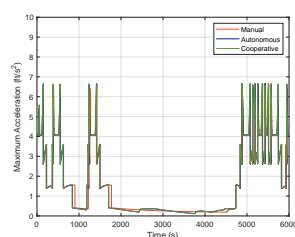
(h) 2002 Chevy Silverado.



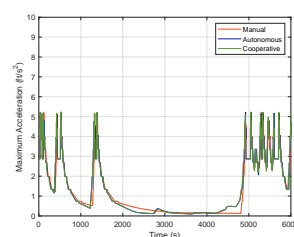
(i) 2008 Chevy Impala.



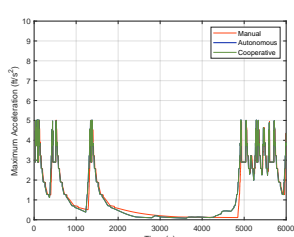
(j) Intermediate semi-trailer.



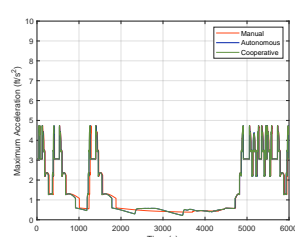
(k) 2004 Chevy Tahoe.



(l) Interstate semi-trailer.

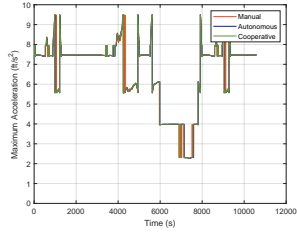


(m) Double semi-trailer.

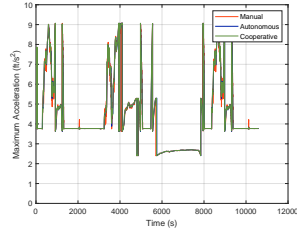


(n) Single-unit truck.

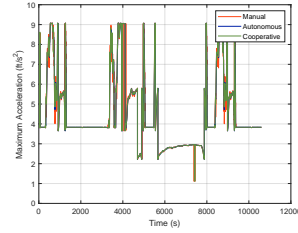
Figure 3: Maximum accelerations over US06 driving schedule.



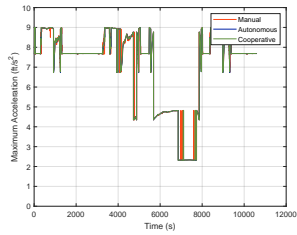
(a) 2011 Ford F150.



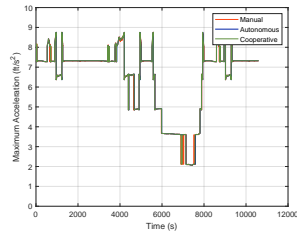
(b) 1998 Buick Century.



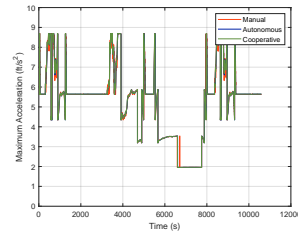
(c) 1998 Chevy S10 Blazer.



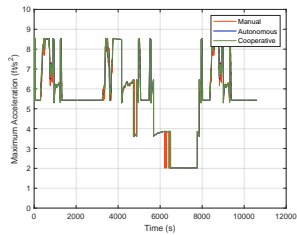
(d) 2004 Pontiac Grand Am.



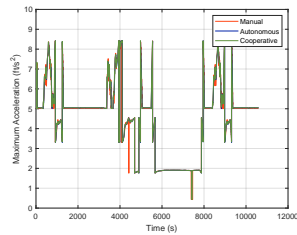
(e) 2006 Honda Civic Si.



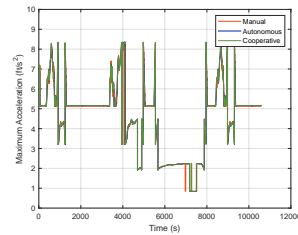
(f) 2005 Mazda 6.



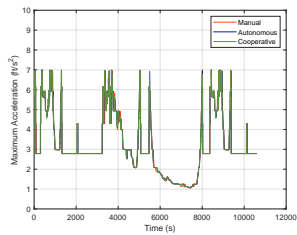
(g) 2009 Honda Civic.



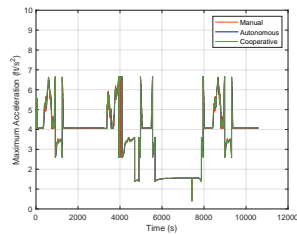
(h) 2002 Chevy Silverado.



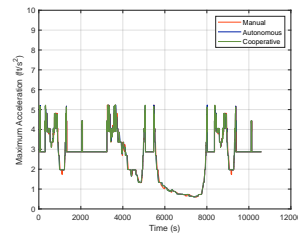
(i) 2008 Chevy Impala.



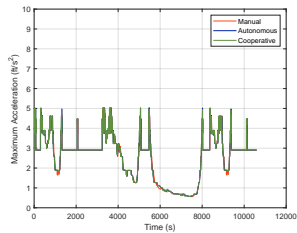
(j) Intermediate semi-trailer.



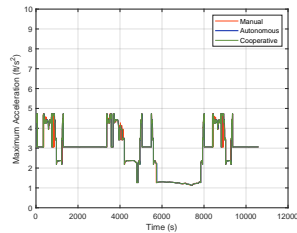
(k) 2004 Chevy Tahoe.



(l) Interstate semi-trailer.

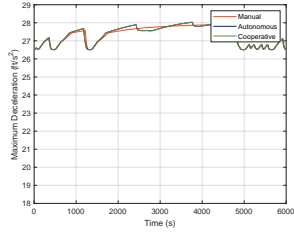


(m) Double semi-trailer.

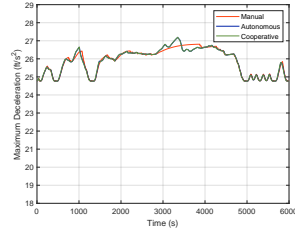


(n) Single-unit truck.

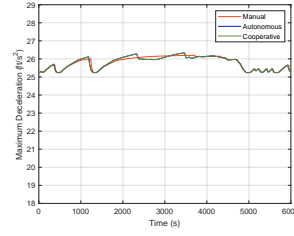
Figure 4: Maximum accelerations over heavy-duty urban dynamometer driving schedule.



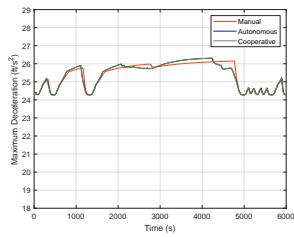
(a) 2004 Chevy Tahoe.



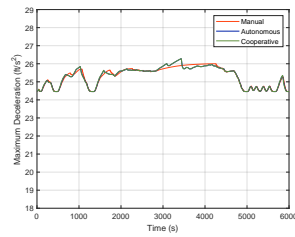
(b) 2011 Ford F150.



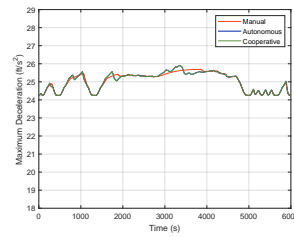
(c) Single-unit truck.



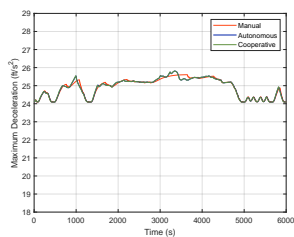
(d) 2002 Chevy Silverado.



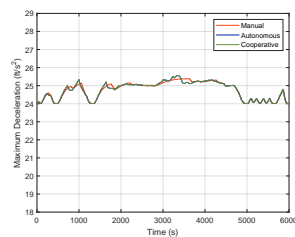
(e) 2009 Honda Civic.



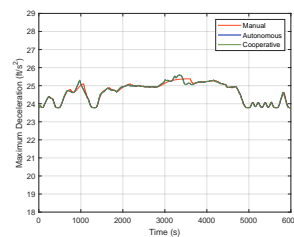
(f) 1998 Chevy S10 Blazer.



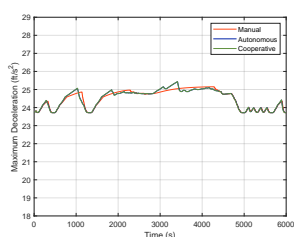
(g) 2006 Honda Civic Si.



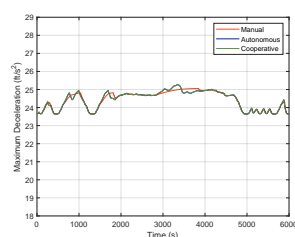
(h) 2005 Mazda 6.



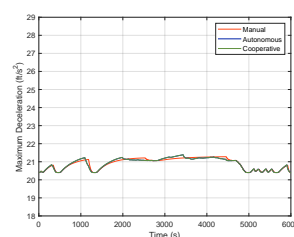
(i) 2004 Pontiac Grand Am.



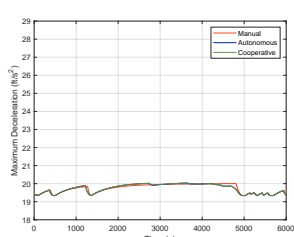
(j) 2008 Chevy Impala.



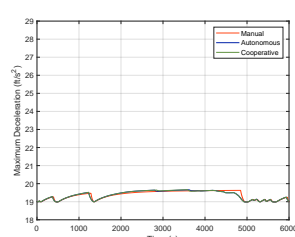
(k) 1998 Buick Century.



(l) Intermediate semi-trailer.

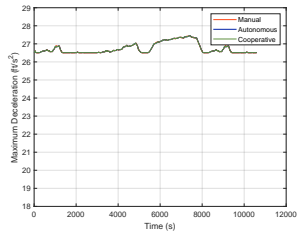


(m) Interstate semi-trailer.

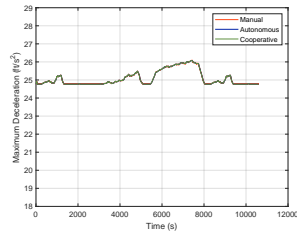


(n) Double semi-trailer.

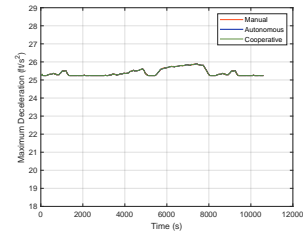
Figure 5: Maximum decelerations over US06 driving schedule.



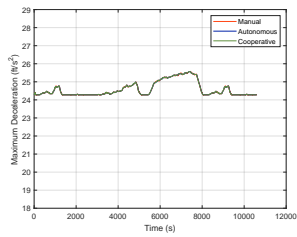
(a) 2004 Chevy Tahoe.



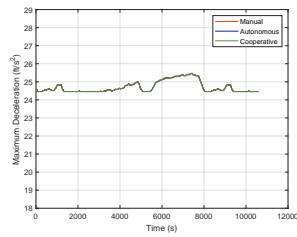
(b) 2011 Ford F150.



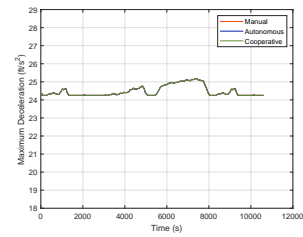
(c) Single-unit truck.



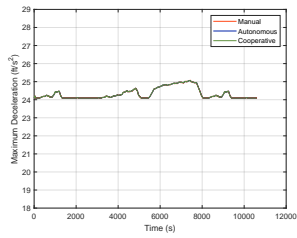
(d) 2002 Chevy Silverado.



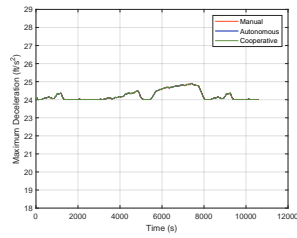
(e) 2009 Honda Civic.



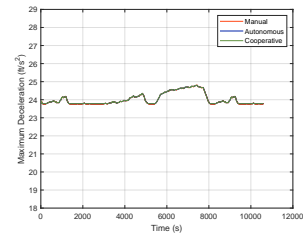
(f) 1998 Chevy S10 Blazer.



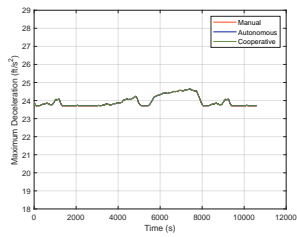
(g) 2006 Honda Civic Si.



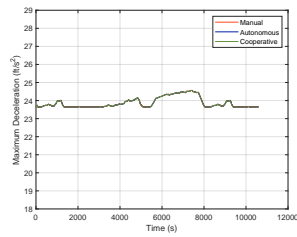
(h) 2005 Mazda 6.



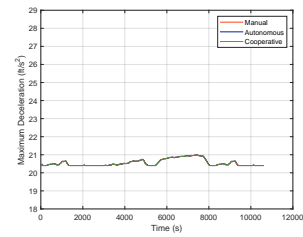
(i) 2004 Pontiac Grand Am.



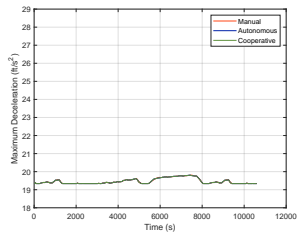
(j) 2008 Chevy Impala.



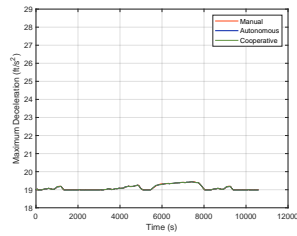
(k) 1998 Buick Century.



(l) Intermediate semi-Trailer.



(m) Interstate semi-Trailer.



(n) Double semi-Trailer.

Figure 6: Maximum decelerations over heavy duty urban dynamometer driving schedule.

Table 3: Peak maximum deceleration values (ft/s²) over US06 and heavy-urban dynamometer driving schedules.

	US06		Cycle D
	Manual	Others*	All Modes**
2004 Chevy Tahoe	27.9	28.0	27.4
2011 Ford F150	26.8	27.2	26.1
Single-Unit Truck	26.2	26.3	25.9
2002 Chevy Silverado	26.1	26.3	25.6
2009 Honda Civic	26.0	26.3	25.5
1998 Chevy S10 Blazer	25.7	25.9	25.2
2006 Honda Civic Si	25.6	25.8	25.1
2005 Mazda 6	25.4	25.6	24.9
2004 Pontiac Grand Am	25.4	25.6	24.8
2008 Chevy Impala	25.2	25.4	24.6
1998 Buick Century	25.1	25.3	24.6
Intermediate Semi-Trailer	21.3	21.4	21.0
Interstate Semi-Trailer	20.0	20.0	19.8
Double Semi-Trailer	19.6	19.7	19.4

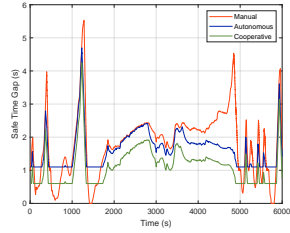
* autonomous and cooperative autonomous modes, ** manual, autonomous, and cooperative autonomous modes.

maximum deceleration value does not change significantly with driving mode and driving schedule (see Table 3), 4) vehicles have equal maximum deceleration in autonomous and cooperative autonomous modes, and 5) trucks have lower maximum deceleration capabilities compared with passenger cars.

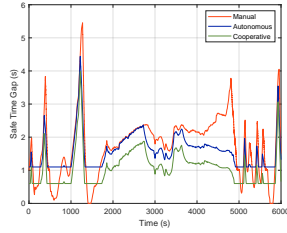
5.5. Minimum Safe Time Gap

Time gaps over US06 and heavy-duty urban dynamometer driving schedules, assuming 2006 Honda Civic Si as leader, are shown in Figure 7 and Figure 8, respectively, arranged from highest to lowest peak time gap value in manual mode over US06 driving schedule—double semi-trailer (5.5 s), interstate semi-trailer (5.5 s), single-unit truck (4.1 s), intermediate semi-trailer (3.9 s), 2004 Chevy Tahoe (3.4 s), 2008 Chevy Impala (2.9 s), 2002 Chevy Silverado (2.8 s), 1998 Chevy S10 Blazer (2.7 s), 1998 Buick Century (2.7 s), 2005 Mazda 6 (2.2 s), 2004 Pontiac Grand Am (2.1 s), 2006 Honda Civic Si (2 s), 2011 Ford F150 (2 s), and 2009 Honda Civic (2 s).

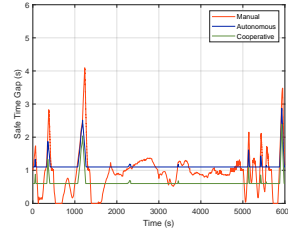
Results show that 1) minimum safe time gap is sensitive to vehicle model and driving schedule, 2) each vehicle model has a considerable range of time gap over US06 driving schedule but not over heavy-duty urban dynamometer driving schedule, 3) peak time gap value changes significantly with driving mode and driving schedule (see Table 4), 4) vehicles maintain longest time gaps in manual mode and shortest time gaps in cooperative autonomous mode, 5) vehicles maintain longer time gaps over US06 driving schedule compared with heavy-duty urban dynamometer driving schedule, 6) trucks should maintain longer time gaps compared with passenger cars, and 7) assuming low constant preset time gaps may result in rear-end crashes, particularly for trucks driving at high speeds. Time gaps in autonomous and cooperative autonomous modes are constant and preset unless constant preset time gaps are less than minimum safe time gaps—in this case, minimum safe time gaps are considered.



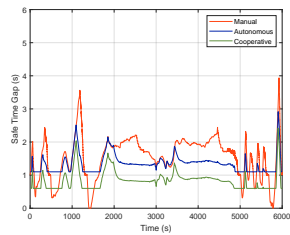
(a) Double semi-trailer.



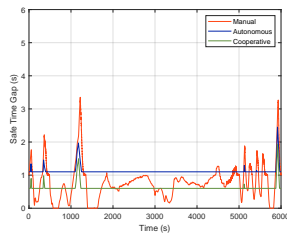
(b) Interstate semi-trailer.



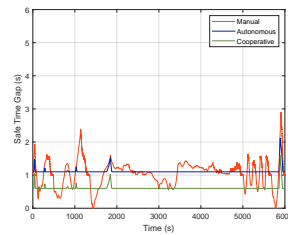
(c) Single-unit truck.



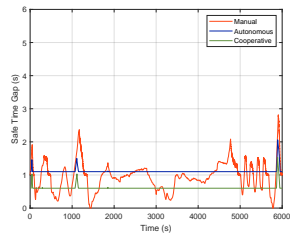
(d) Intermediate semi-trailer.



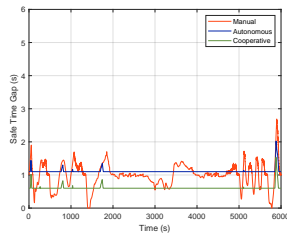
(e) 2004 Chevy Tahoe.



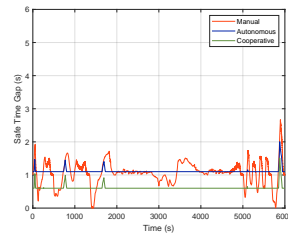
(f) 2008 Chevy Impala.



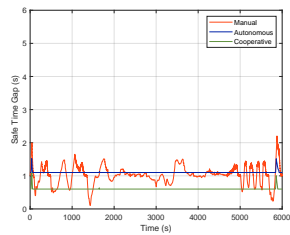
(g) 2002 Chevy Silverado.



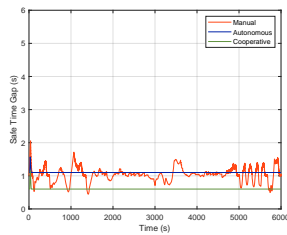
(h) 1998 Chevy S10 Blazer.



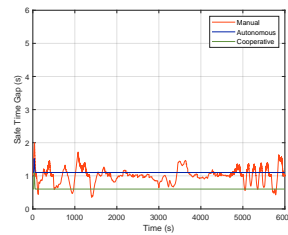
(i) 1998 Buick Century.



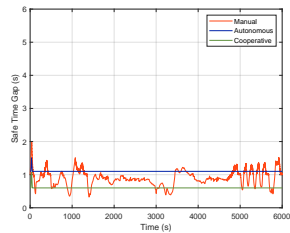
(j) 2005 Mazda 6.



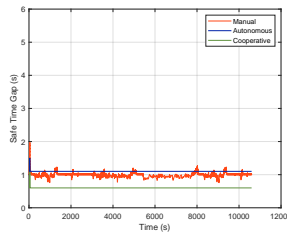
(k) 2004 Pontiac Grand Am.



(l) 2006 Honda Civic Si.

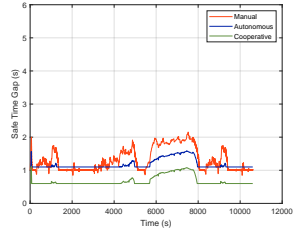


(m) 2011 Ford F150.

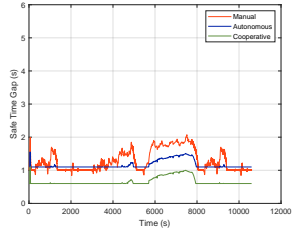


(n) 2009 Honda Civic.

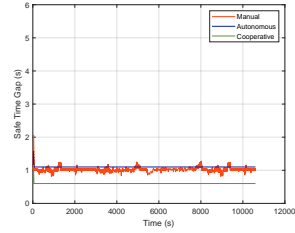
Figure 7: Time gaps over US06 driving schedule.



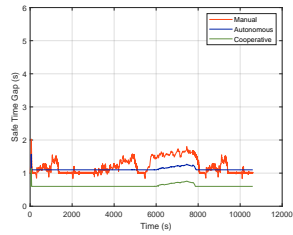
(a) Double semi-trailer.



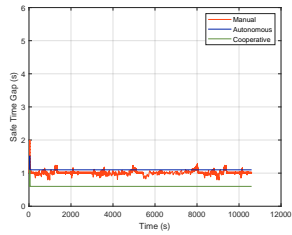
(b) Interstate semi-trailer.



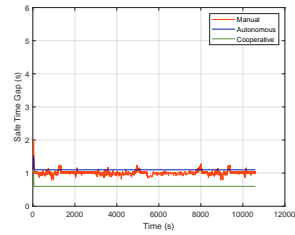
(c) 2004 Pontiac Grand Am.



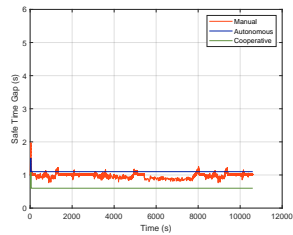
(d) Intermediate semi-trailer.



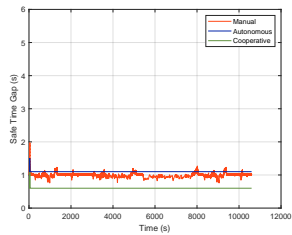
(e) 2005 Mazda 6.



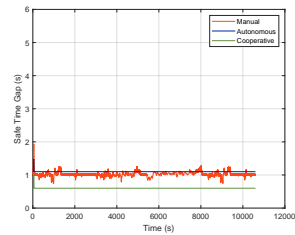
(f) 2006 Honda Civic Si.



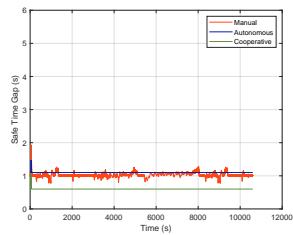
(g) 2011 Ford F150.



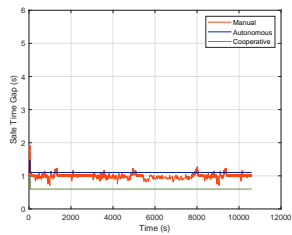
(h) 2009 Honda Civic.



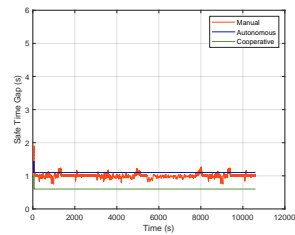
(i) 2008 Chevy Impala.



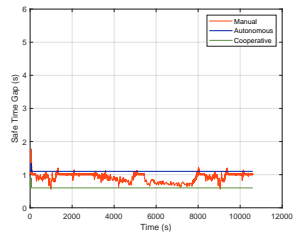
(j) 1998 Buick Century.



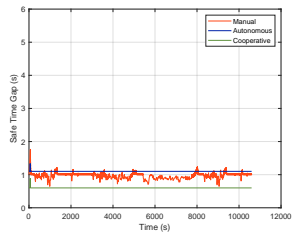
(k) 2002 Chevy Silverado.



(l) 1998 Chevy S10 Blazer.

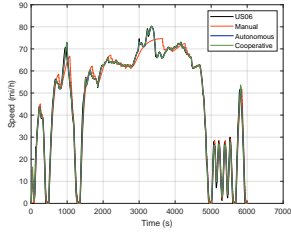


(m) 2004 Chevy Tahoe.

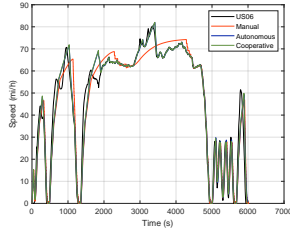


(n) Single-unit truck.

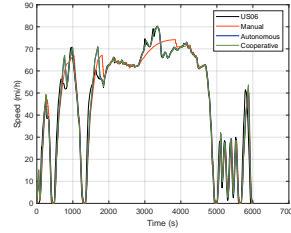
Figure 8: Time gaps over heavy-duty urban dynamometer driving schedule.



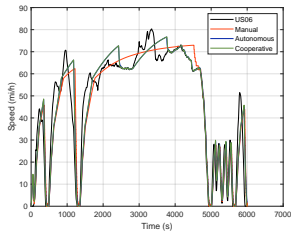
(a) 2006 Honda Civic Si.



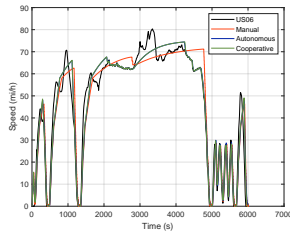
(b) 2008 Chevy Impala.



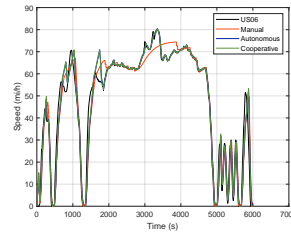
(c) 1998 Buick Century.



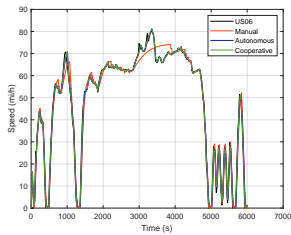
(d) 2004 Chevy Tahoe.



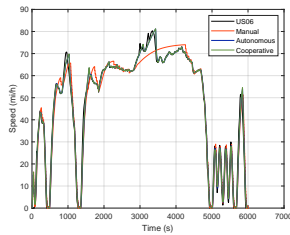
(e) 2002 Chevy Silverado.



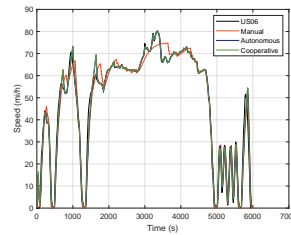
(f) 1998 Chevy S10 Blazer.



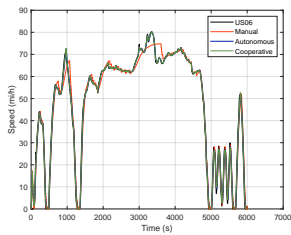
(g) 2011 Ford F150.



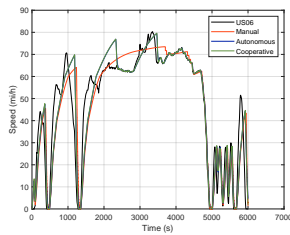
(h) 2009 Honda Civic.



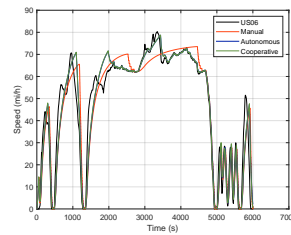
(i) 2005 Mazda 6.



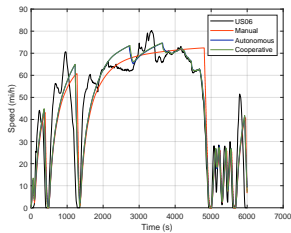
(j) 2004 Pontiac Grand Am.



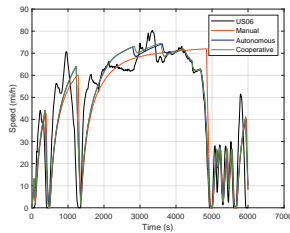
(k) Single-unit truck.



(l) Intermediate semi-trailer.

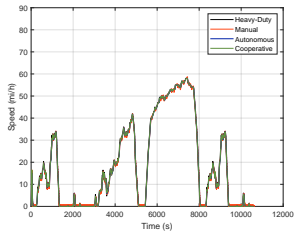


(m) Interstate semi-trailer.

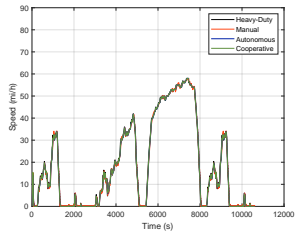


(n) Double semi-trailer.

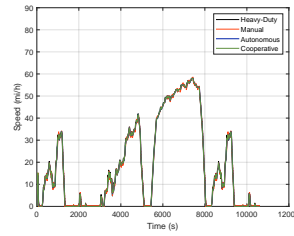
Figure 9: Speed profiles for US06 driving schedule.



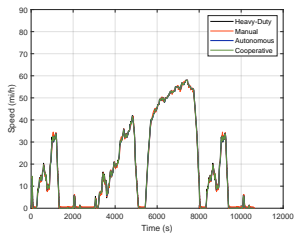
(a) 2006 Honda Civic Si.



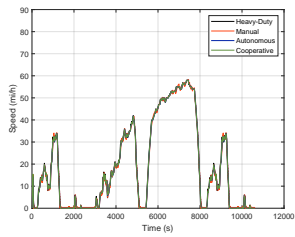
(b) 2008 Chevy Impala.



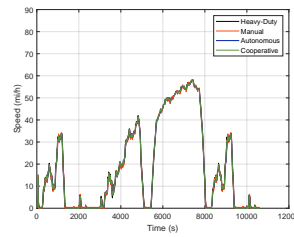
(c) 1998 Buick Century.



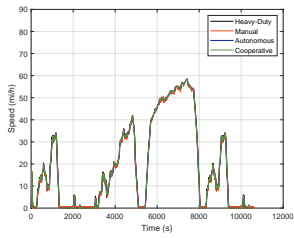
(d) 2004 Chevy Tahoe.



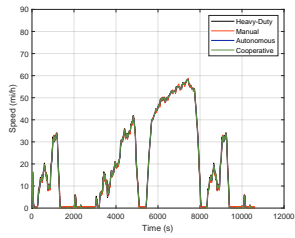
(e) 2002 Chevy Silverado.



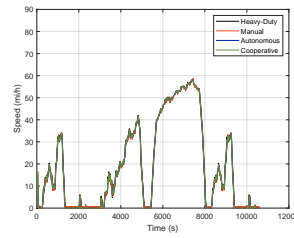
(f) 1998 Chevy S10 Blazer.



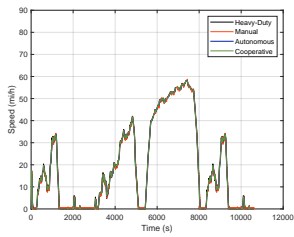
(g) 2011 Ford F150.



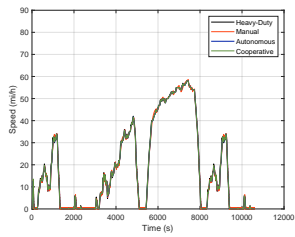
(h) 2009 Honda Civic.



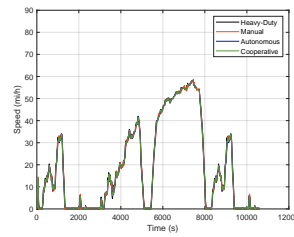
(i) 2005 Mazda 6.



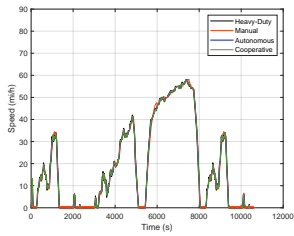
(j) 2004 Pontiac Grand Am.



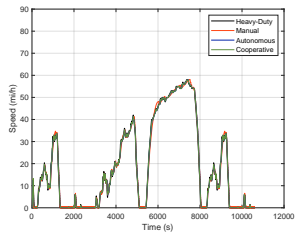
(k) Single-unit truck.



(l) Intermediate semi-trailer.



(m) Interstate semi-trailer.



(n) Double semi-trailer.

Figure 10: Speed profiles over heavy-duty urban dynamometer driving schedule.

Table 4: Peak time gap values (s) over US06 and heavy-urban dynamometer driving schedules.

	Manual		Autonomous		Cooperative	
	US06	Cycle D	US06	Cycle D	US06	Cycle D
Double Semi-Trailer	5.5	4.7	4.2	2.2	1.6	1.1
Interstate Semi-Trailer	5.5	4.4	4.0	2.1	1.6	1.1
Single-Unit Truck	4.1	2.9	2.4	1.8	1.3	0.9
Intermediate Semi-Trailer	3.9	2.9	2.4	2.0	1.6	1.1
2004 Chevy Tahoe	3.4	2.5	1.9	1.8	1.3	0.9
2008 Chevy Impala	2.9	2.1	1.6	1.9	1.5	1.0
2002 Chevy Silverado	2.8	2.1	1.5	1.9	1.5	1.0
1998 Chevy S10 Blazer	2.7	2.0	1.5	1.9	1.4	1.0
1998 Buick Century	2.7	2.0	1.5	1.9	1.5	1.0
2005 Mazda 6	2.2	1.5	1.1	2.0	1.5	1.1
2004 Pontiac Grand Am	2.1	1.6	1.2	2.1	1.6	1.2
2006 Honda Civic Si	2.0	1.5	1.1	2.0	1.5	1.1
2011 Ford F150	2.0	1.5	1.1	2.0	1.5	1.1
2009 Honda Civic	2.0	1.5	1.1	2.0	1.5	1.1

5.6. Speed Profile

Speed profiles over US06 and heavy-duty urban dynamometer driving schedules, assuming 2006 Honda Civic Si as leader, are shown in Figure 9 and Figure 10, respectively. Results show that 1) designed longitudinal controllers are more efficient for vehicles over heavy-duty urban dynamometer driving schedule compared with US06 driving schedule, 2) vehicles have equal speed in autonomous and cooperative autonomous modes, and 3) reducing controller coefficients, particularly over US06 driving schedule and at beginning of simulation, enhanced driver experience—reduced vertical oscillations—but increased steady-state error.

6. Summary/Future Work

There is a considerable gap between real-world limitations of vehicles and assumptions of mechanical/physics underpinnings of simulation models. This paper proposes a vehicle-following model for human-driven vehicles and longitudinal control functions for autonomous and cooperative autonomous vehicles, considering driver characteristics and vehicle dynamics in calculated accelerations, decelerations, distance gaps, time gaps, and speeds. Unlike conventional longitudinal control functions that rely on constant preset time gaps and constant controller coefficients, proposed longitudinal control functions consider dynamic time gaps and dynamic controller coefficients, designed in a way to minimize settling time and overshoot while not compromising safety.

It can be concluded from this paper that 1) maximum acceleration and maximum deceleration are specific to vehicle model and driving schedule, 2) peak maximum acceleration and maximum deceleration values do not change significantly with driving mode and driving schedule, 3) peak time gap value changes significantly with driving mode and driving schedule, 4) constant preset time gap should be checked with minimum safe time gap at each simulation time step, particularly for trucks driving at high speeds, to ensure there would be no rear-end crashes, and 5)

there is always a trade-off between increasing driver comfort and reducing steady-state error in designing longitudinal control functions.

This paper assumed vehicles drive in a single lane, and there is no cut-in or cut-out maneuver. However, a lateral maneuver can temporarily affect longitudinal behaviors of vehicles, consequently affecting macroscopic measures of traffic flow. Vehicles temporarily adopt longer time gaps before a lane-change maneuver and temporarily accept shorter time gaps after each lane-change maneuver. Future work can estimate the macroscopic benefits of cooperative autonomous vehicles for different flow rates, market penetrations, and types of facilities.

7. Appendix

Proposed traffic microsimulation tool contains ten driver types—type 1-most conservative driver and type 10-most aggressive driver, treating drivers as distinct objects, enabling users to customize vehicle and driver characteristics separately. Each driver type should be associated with multipliers for acceleration, deceleration, and speed (see Table 5).

Each vehicle model is assigned to only one fleet type—small auto, large auto, small truck, and large truck—and an FHWA (Federal Highway Administration) classification with physical, engine, transmission, and drivetrain properties (see Table 6 through Table 13).

This paper includes four truck configurations: single-unit truck, intermediate semi-trailer, interstate semi-trailer, and double semi-trailer. PACCAR PX-7 engine with an HP-Torque rating of 300 HP/660 lb-ft is used for single-unit trucks and PACCAR MX-13 engines with an HP-Torque rating of 485 HP/1650 lb-ft is used for other three truck configurations.

Vehicle IDs 1 through 14 correspond to 2006 Honda Civic Si, 2008 Chevy Impala, 1998 Buick Century, 2004 Chevy Tahoe, 2002 Chevy Silverado, 1998 Chevy S10 Blazer, 2011 Ford F150, 2009 Honda Civic, 2005 Mazda 6, 2004 Pontiac Grand Am, single-unit truck, intermediate semi-trailer, interstate semi-trailer, and double semi-trailer, respectively.

References

Ahn, K., Rakha, H., Trani, A., Van Aerde, M., 2002. Estimating vehicle fuel consumption and emissions based on instantaneous speed and acceleration levels. *Journal of transportation engineering* 128, 182–190.

Table 5: Default values for driver characteristics (SwashSim, 2019a).

Driver ID	Speed Multiplier	Acceleration Multiplier	Deceleration Multiplier	% in Traffic
1	0.910	0.875	0.950	5
2	0.930	0.900	0.960	8
3	0.950	0.925	0.970	10
4	0.970	0.950	0.980	12
5	1.000	0.975	0.990	15
6	1.025	1.000	1.000	15
7	1.050	1.050	1.010	12
8	1.075	1.075	1.020	10
9	1.100	1.100	1.030	8
10	1.120	1.125	1.040	5

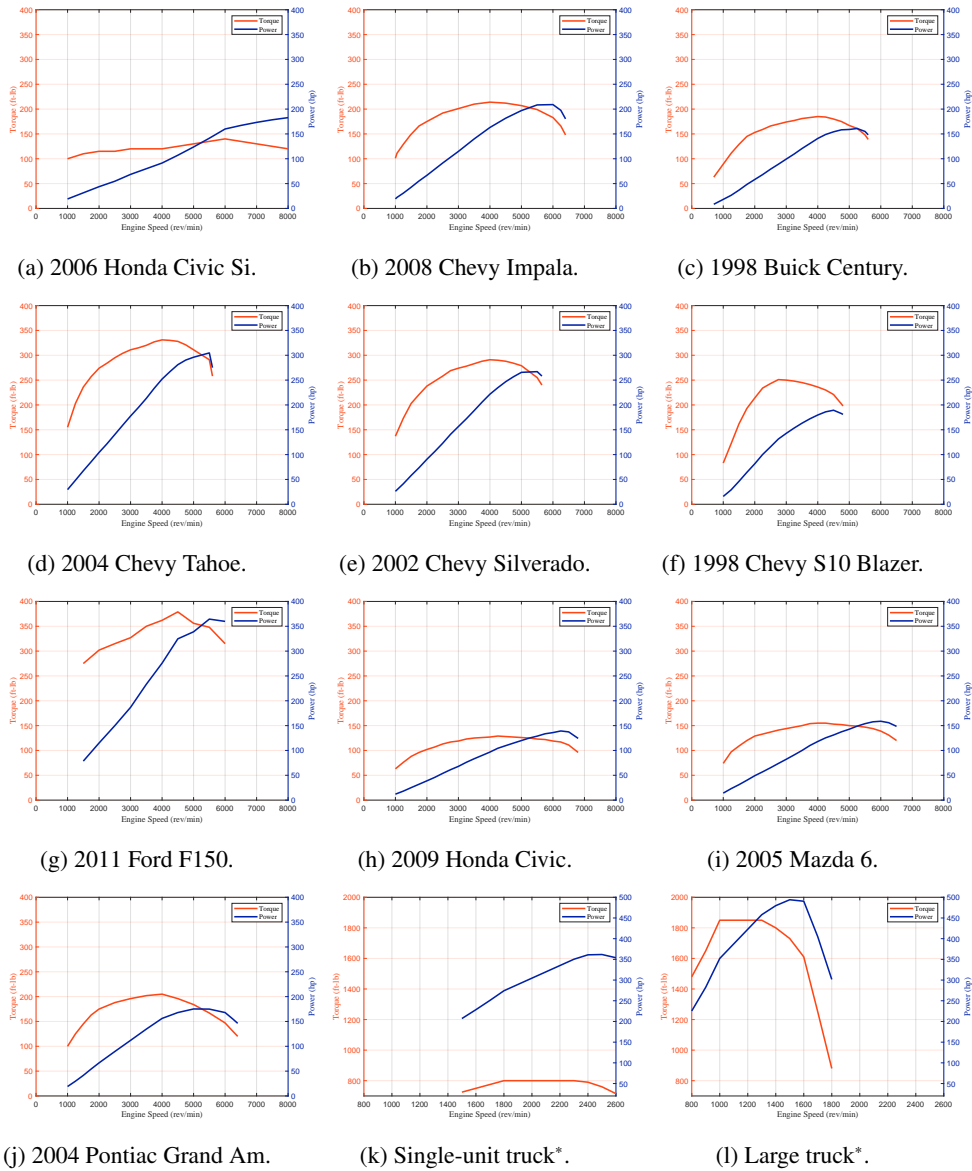


Figure 11: Torque maps included.

* have different plot scales.

Table 6: Physical properties of vehicles included-part 1 (SwashSim, 2019b).

Vehicle ID	1	2	3	4	5	6	7
fleet Type	Auto*	Auto*	Auto*	Auto**	Auto**	Auto**	Auto**
FHWA Classification	2	2	2	3	3	2	3
Length (ft)	14.57	16.70	16.22	16.40	18.98	16.94	19.31
Width (ft)	5.740	6.100	6.060	6.575	6.540	6.658	6.575
Height (ft)	4.460	4.900	4.720	6.358	5.930	5.275	6.350
Weight (lb)	3060	3756	3553	7000	5100	4800	5200
Wheel Radius (ft)	1.03	1.11	1.10	1.28	1.24	1.13	1.29
Drag Coefficient	0.33	0.33	0.32	0.43	0.52	0.42	0.50

* small, ** large.

Table 7: Physical properties of vehicles included-part 2 (SwashSim, 2019b).

Vehicle ID	8	9	10	11	12	13	14
Fleet Type	Auto*	Auto*	Auto*	Truck*	Truck**	Truck**	Truck**
FHWA Classification	2	2	2	5	8	9	12
Length (ft)	14.78	15.57	15.53	29.00	55.00	68.50	74.60
Width (ft)	5.750	5.840	5.870	7.000	8.000	8.000	8.000
Height (ft)	4.708	4.725	4.592	10.000	10.000	10.000	10.000
Weight (lb)	3020	3521	3300	25000	37000	53000	55000
Wheel Radius (ft)	1.04	1.06	1.04	1.66	1.66	1.66	1.66
Drag Coefficient	0.32	0.31	0.36	0.55	0.66	0.66	0.66

* small, ** large.

Table 8: Engines included-part 1 (SwashSim, 2019b).

Vehicle ID	1	2	3	4	5	6
Displacement	2	4	3	5	5	4
Engine Idle Speed (revs/min)	1000	1000	700	1000	1000	1000
Maximum Engine Speed (revs/min)	8000	6400	5800	5600	5650	4800

Table 9: Engines included-part 2 (SwashSim, 2019b).

Vehicle ID	7	8	9	10	11	12,13,14
Displacement	5	2	2	3	7	12
Engine Idle Speed (revs/min)	1500	1000	1000	1000	700	800
Maximum Engine Speed (revs/min)	6000	6800	6500	6400	2600	2200

Table 10: Transmissions included-part 1 (SwashSim, 2019b).

Vehicle ID	1	2	3	4	5	6
Drive Axle Slippage	0.05	0.05	0.05	0.05	0.05	0.05
Drivetrain Efficiency	0.92	0.92	0.90	0.90	0.90	0.90
Differential Gear Ratio	4.770	2.860	3.290	3.230	3.230	3.420

Table 11: Transmissions included-part 2 (SwashSim, 2019b).

Vehicle ID	7	8	9	10	11	12,13,14
Drive Axle Slippage	0.05	0.03	0.03	0.04	0.05	0.05
Drivetrain Efficiency	0.92	0.94	0.94	0.93	0.80	0.80
Differential Gear Ratio	3.550	4.437	4.147	3.750	4.400	3.500

Table 12: Drivetrains—gear ratio/shift up speed/shift down speed (mi/h)—included-part 1 (SwashSim, 2019b).

Vehicle ID	1	2	3	4,5,6	7
Gear 1	3.27/0/15	2.92/0/20	2.92/0/20	3.06/0/20	4.17/0/15
Gear 2	2.13/10/25	1.57/18/36	1.57/18/40	1.63/18/36	2.34/12/30
Gear 3	1.52/20/35	1.00/32/56	1.00/36/65	1.00/32/58	1.52/26/45
Gear 4	1.15/30/45	0.71/52/110	0.71/52/110	0.70/52/110	1.14/40/55
Gear 5	0.92/40/55	NA	NA	NA	0.86/50/65
Gear 6	0.66/50/110	NA	NA	NA	0.69/60/110

Table 13: Drivetrains—gear ratio/shift up speed/shift down speed (mi/h)—included-part 2 (SwashSim, 2019b).

Vehicle ID	8	9	10	11	12,13,14
Gear 1	2.67/0/22	2.82/0/18	2.96/0/20	7.59/0/9	11.06/0/5
Gear 2	1.53/18/38	1.50/15/36	1.62/16/38	5.06/6/13	8.20/3/7
Gear 3	1.02/34/50	1.00/32/52	1.00/34/54	3.38/10/20	6.06/5/10
Gear 4	0.72/46/65	0.73/46/110	0.68/50/110	2.25/17/26	4.49/7/14
Gear 5	0.53/60/110	NA	NA	1.50/22/40	3.32/10/19
Gear 6	NA	NA	NA	1.00/35/60	2.46/13/25
Gear 7	NA	NA	NA	0.75/55/110	1.82/20/34
Gear 8	NA	NA	NA	NA	1.35/30/43
Gear 9	NA	NA	NA	NA	1.00/38/55
Gear 10	NA	NA	NA	NA	0.74/50/110

- Aimsun, 2019. Aimsun unveils new platform for simulating a driverless future. <https://www.aimsun.com/aimsun-auto-launch/>.
- Akçelik, R., Besley, M., 2001. Acceleration and deceleration models, in: 23rd Conference of Australian Institutes of Transport Research (CAITR 2001), Monash University, Melbourne, Australia, p. 12.
- Amoozadeh, M., Deng, H., Chuah, C.N., Zhang, H.M., Ghosal, D., 2015. Platoon management with cooperative adaptive cruise control enabled by vanet. *Vehicular communications* 2, 110–123.
- Anyu, A.R., Roupail, N.M., Frey, H.C., Schroeder, B., 2014. Application of aimsun microsimulation model to estimate emissions on signalized arterial corridors. *Transportation Research Record* 2428, 75–86.
- Arasan, V.T., Koshy, R.Z., 2005. Methodology for modeling highly heterogeneous traffic flow. *Journal of Transportation Engineering* 131, 544–551.
- Arem, B.v., Driever, J., Feenstra, P., Ploeg, J., Klunder, G., Wilmink, I., Zoutendijk, A., Papp, Z., Netten, B., 2007. Design and evaluation of an integrated full-range speed assistant. Technical Report. TNO.
- Arem, B.V., Van Driel, C.J., Visser, R., 2006. The impact of cooperative adaptive cruise control on traffic-flow characteristics. *IEEE Transactions on intelligent transportation systems* 7, 429–436.
- Bokare, P., Maurya, A., 2017. Acceleration-deceleration behaviour of various vehicle types. *Transportation research procedia* 25, 4733–4749.
- Desiraju, D., Chantem, T., Heaslip, K., 2014. Minimizing the disruption of traffic flow of automated vehicles during lane changes. *IEEE Transactions on Intelligent Transportation Systems* 16, 1249–1258.
- EPA, 2017. Dynamometer drive schedules. <https://www.epa.gov/vehicle-and-fuel-emissions-testing/>

- dynamometer-drive-schedules.
- Fang, F.C., Elefteriadou, L., 2005. Some guidelines for selecting microsimulation models for interchange traffic operational analysis. *Journal of Transportation Engineering* 131, 535–543.
- Guo, T., 2017. Cooperative adaptive cruise control (CACC) in the context of vehicle to vehicle communications: an overview. Technical Report. Institute of Transportation Studies UC Davis.
- Kuriyama, M., Yamamoto, S., Miyatake, M., 2010. Theoretical study on eco-driving technique for an electric vehicle with dynamic programming, in: 2010 International Conference on Electrical Machines and Systems, IEEE. pp. 2026–2030.
- Lee, J., Park, B., 2012. Development and evaluation of a cooperative vehicle intersection control algorithm under the connected vehicles environment. *IEEE Transactions on Intelligent Transportation Systems* 13, 81–90.
- Lee, J., Park, B.B., Malakorn, K., So, J.J., 2013. Sustainability assessments of cooperative vehicle intersection control at an urban corridor. *Transportation Research Part C: Emerging Technologies* 32, 193–206.
- Lemessi, M., 2001. An slx-based microsimulation model for a two-lane road section, in: *Proceeding of the 2001 Winter Simulation Conference* (Cat. No. 01CH37304), IEEE. pp. 1064–1071.
- Li, Z., Elefteriadou, L., Ranka, S., 2014. Signal control optimization for automated vehicles at isolated signalized intersections. *Transportation Research Part C: Emerging Technologies* 49, 1–18.
- Liu, H., Kan, X.D., Shladover, S.E., Lu, X.Y., Ferlis, R.E., 2018. Modeling impacts of cooperative adaptive cruise control on mixed traffic flow in multi-lane freeway facilities. *Transportation Research Part C: Emerging Technologies* 95, 261–279.
- Lu, X.Y., Lee, J., Chen, D., Bared, J., Dailey, D., Shladover, S.E., 2014. Freeway micro-simulation calibration: case study using aimsun and vissim with detailed field data. *Transportation Research Board*.
- Manning, F.L., Washburn, S.S., 2019. *Principles of Highway Engineering and Traffic Analysis*. John Wiley & Sons, Hoboken, NJ.
- Maurya, A.K., Bokare, P.S., 2012. Study of deceleration behaviour of different vehicle types. *International Journal for Traffic & Transport Engineering* 2.
- Milanés, V., Shladover, S.E., Spring, J., Nowakowski, C., Kawazoe, H., Nakamura, M., 2013. Cooperative adaptive cruise control in real traffic situations. *IEEE Transactions on Intelligent Transportation Systems* 15, 296–305.
- NHTSA, 2017. Federal motor vehicle safety standards; v2v communications. *Federal Register* 82, 3854–4019.
- NHTSA, 2018a. Critical reasons for crashes investigated in the national motor vehicle crash causation survey (traffic safety facts). Technical Report DOT HS 812 506. USDOT.
- NHTSA, 2018b. Summary of motor vehicle crashes: 2016 data (traffic safety facts). Technical Report DOT HS 812 580. USDOT.
- NHTSA, 2019. Automated Vehicles for Safety. <https://www.nhtsa.gov/technology-innovation/automated-vehicles-safety>.
- PTV Vissim, 2019. Virtual testing of autonomous vehicles with PTV vissim. <https://www.ptvgroup.com/en/solutions/products/ptv-vissim/areas-of-application/autonomous-vehicles-and-new-mobility/>.
- Rakha, H., Ding, Y., 2003. Impact of stops on vehicle fuel consumption and emissions. *Journal of Transportation Engineering* 129, 23–32.
- Rakha, H., Lucic, I., 2002. Variable power vehicle dynamics model for estimating truck accelerations. *Journal of transportation engineering* 128, 412–419.
- Rakha, H., Snare, M., Dion, F., 2004. Vehicle dynamics model for estimating maximum light-duty vehicle acceleration levels. *Transportation Research Record* 1883, 40–49.
- Ramezani, H., Shladover, S.E., Lu, X.Y., Altan, O.D., 2018. Micro-simulation of truck platooning with cooperative adaptive cruise control: Model development and a case study. *Transportation Research Record* 2672, 55–65.
- Shladover, S.E., Su, D., Lu, X.Y., 2012. Impacts of cooperative adaptive cruise control on freeway traffic flow. *Transportation Research Record* 2324, 63–70.
- Song, G., Yu, L., Zhang, Y., 2012. Applicability of traffic microsimulation models in vehicle emissions estimates: case study of vissim. *Transportation Research Record* 2270, 132–141.
- SwashSim, 2019a. Drivers. <https://swashsim.miraheze.org/wiki/Drivers>.
- SwashSim, 2019b. Vehicles. <https://swashsim.miraheze.org/wiki/Vehicles>.
- Tian, J., Jiang, R., Li, G., Treiber, M., Zhu, C., Jia, B., 2016. Improved 2d intelligent driver model simulating synchronized flow and evolution concavity in traffic flow. arXiv preprint arXiv:1603.00264.
- Wang, X.Y., Liu, J.S., 2005. Research of the lane utilization with microsimulation, in: 2005 International Conference on Machine Learning and Cybernetics, IEEE. pp. 2681–2687.
- Zhu, M., Wang, X., Tarko, A., et al., 2018. Modeling car-following behavior on urban expressways in shanghai: A naturalistic driving study. *Transportation research part C: emerging technologies* 93, 425–445.